Supplementary Material

This document contains seven sections, which include comparisons to literature threshold energies and, with the exception of H_2–loss reactions, depictions of the B2GP-PLYP-D3/def2-TZVP optimised first order saddle points for the given reaction:

S1 Possible S_0 reactions for butanal.

S2 Decarbonylation reactions

S3 Concerted triple fragmentation reactions

S4 Norrish Type III (β-H transfer) reactions

S5 H_2–loss reactions

S6 Alkane/alkene elimination

S7 Keto–enol tautomerisation

Cartesian coordinates for all optimised first-order saddle point geometries are provided as text files in a ZIP folder.

S1 Possible S_0 reactions for butanal

Threshold energies for seven of the S_0 unimolecular reactions considered here are illustrated for butanal in Fig. S1. Butanal is sufficiently large to have all three possible H_2–loss channels, but enal–ketene isomerisation is only available to the α,β-unsaturated aldehydes and dissociation to an alkane and a ketene is available only to ketones. Schematic mechanisms are shown for concerted triple fragmentation (TF), which leads to propene, H_2 and CO products, and Norrish Type III dissociation (NTIII), which involves a 4-centre β-hydrogen transfer that forms propene and formaldehyde.

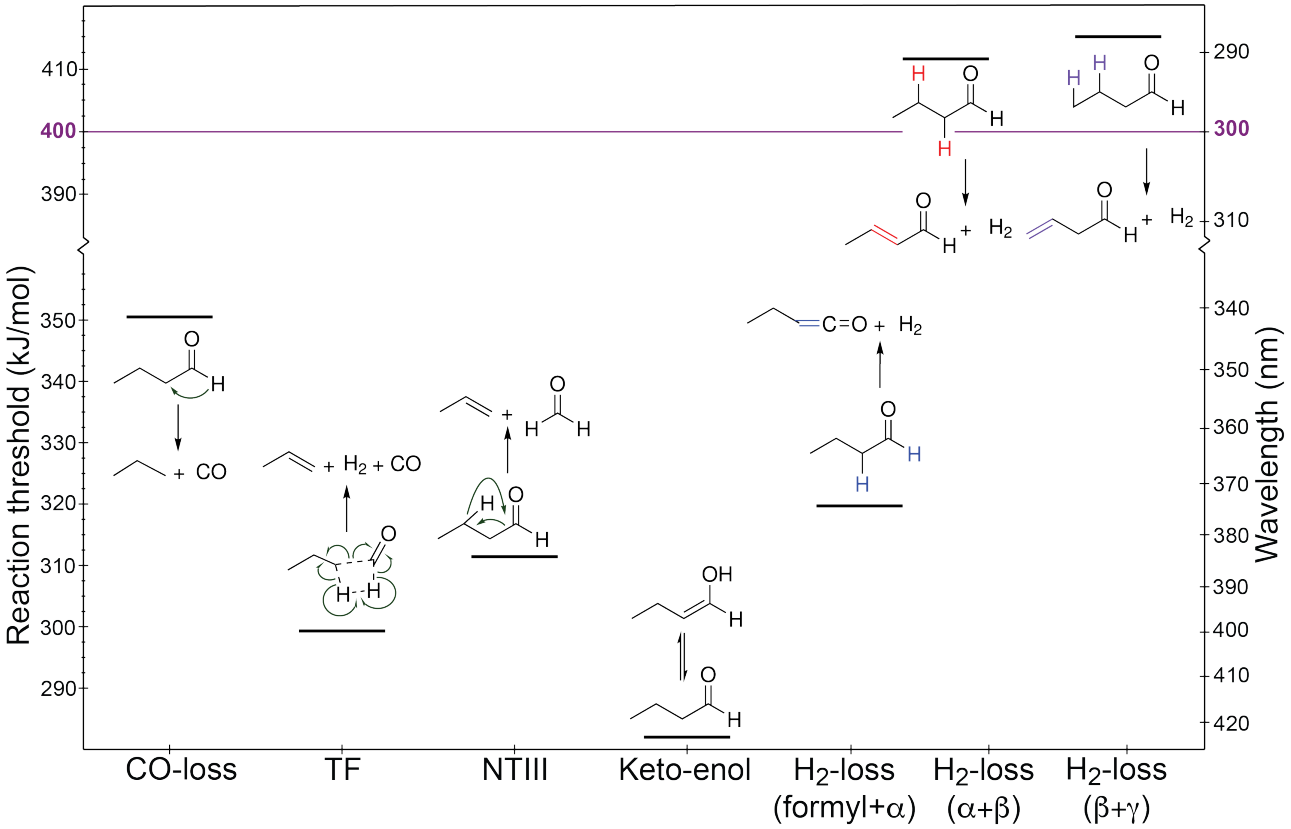

Figure S1: Zero-point vibrational energy corrected B2GP-PLYP-D3/def2-TZVP S_0 thresholds for butanal, as indicated. The maximum energy available in the troposphere (400 kJ/mol) is indicated as a purple line.

As shown in Fig. S1, and common to all aliphatic carbonyls considered, the lowest energy threshold is for keto–enol isomerisation, although this reaction is reversible. The lowest energy dissociation channels are TF, NTIII and then (formyl + α) H_2–loss. Direct decarbonylation (and NTI dissociation, which is not shown in the figure) occur at higher energy and the two other H_2–loss channels have thresholds above the actinic energy range.

S2 Decarbonylation reactions

Decarbonylation reactions have been studied theoretically for a number of carbonyls in the dataset. Selected high-level literature results are compared to our B2GP-PLYP-D3/def2-TZVP calculations in Table S1.

The B2GP-PLYP-D3/def2-TZVP first-order saddle points, representing transition states (TSs) for the S_0 direct decarbonylation reaction, are shown in Figs S2 and S3. Key geometric parameters, in Å and degrees, are also shown in the figures. Although conceivable in any carbonyl, no TSs for direct decarbonylation were found for any ketone in the dataset, or for diacetyl.

With the exception of formaldehyde, which is known to be problematic, for example, Feller et al. (2000), our calculations compare well with the previous literature. The results in Table S1 indicate that electron correlation is important in the accurate description of the saddle point and an accurate saddle point geometry is required for single-point energies. For example, in propanal, the CASPT2 threshold, determined using CASSCF(6,6) geometries, does not appear to be as reliable as the single-point CCSD(T) calculations (Tsai et al., 2014). The MP2/6-31+G(d) calculations of Koch et al. (2001) on glyoxal also appear unreliable. With the exception of formaldehyde and the CASPT2 and MP2 results, the root-mean-square deviation of our calculated B2GP-PLYP-D3/def2-TZVP decarbonylation thresholds to those in Table S1 is less than 6 kJ/mol, consistent with previous assessments of the method (Karton et al., 2008; Rowell et al., 2019).

A number of decarbonylation pathways have been reported for glyoxal (Koch et al., 2001; Chin and Lee, 2012). The two C=O groups in glyoxal can be initially *cis* or *trans*, with *trans* glyoxal ∼18 kJ/mol lower in energy (Ruscic, B. and Bross, D. H., 2020; Ruscic et al., 2005). We have optimised three first-order saddle points for glyoxal decarbonylation to form formaldehyde, H_2CO and CO. These are illustrated in Fig. S3. The lowest energy TS is non-planar, as shown in Fig. S3a, corresponding to a threshold energy of 225 kJ/mol. There are two planar TS, with *cis* and *trans* configurations, as shown in Figs S3b and S3c, with thresholds of 328 and 320 kJ/mol, respectively. Decarbonylation from *trans*-glyoxal can also form hydroxymethylene, HOCH, as shown in Fig. S3c, with a threshold of 251 kJ/mol. As shown in Table S1, our B2GP-PLYP-D3 calculations agree well with previous high-level G3, CBS-APNO and CCSD(T) results, although we predict the planar *trans* TS to H_2CO + CO to be 8 kJ/mol lower in energy than the planar *cis* TS, contradicting the G3 and MP2 results of Koch et al. (2001).

Table S1: Comparison of calculated zero-point vibrational energy corrected S_0 thresholds (kJ/mol) for decarbonylation reactions.

Species and Method[a]	Threshold	Reference
Formaldehyde:		
Experiment	331.4	Polik et al. (1990)
B2GP-PYLP-D3/def2-TZVP	352	This work
CCSD(T)/CBS+CV//CCSD/apVDZ	340.6	Feller et al. (2000)
(8e,8o)-CAS+1+2+QC/apVQZ//(8e,8o)-CASPT2/apVTZ	336.8	Harding et al. (2007)
RCCSD(T)/apVQZ//RCCSD(T)/apVTZ	339.7	Harding et al. (2007)
Acetaldehyde:		
B2GP-PYLP-D3/def2-TZVP	352	This work
G2	246.9	Martell et al. (1997)
CBS-QB3	350.6	Nguyen et al. (2005)
G3	347.7	Nguyen et al. (2005)
(8e,7o)-CAS+1+2+QC/apVQZ//(8e,8o)-CASPT2/apVTZ	347.3	Harding et al. (2007)
RCCSD(T)/apVQZ//RCCSD(T)/apVTZ	343.1	Harding et al. (2007)
CCSD(T)/pVTZ//B3LYP/6-311++G(d,p)	347.4	Yang et al. (2007)
Propanal:		
B2GP-PLYP-D3/def2-TZVP	348	This work
(10e,9o)-CASPT2/6-311++G(d,p)//CASSCF(6,6)/6-311++G(d,p)	315.9	Tsai et al. (2014)
CCSD(T)/6-311++G(d,p)//CASSCF(6,6)/6-311++G(d,p)	350.4	Tsai et al. (2014)
CCSD(T)/6-311+G(3df,2p)//B3LYP/6-311G(d,p)	350.2	Chin and Lee (2012)
Acrolein:		
B2GP-PLYP-D3/def2-TZVP	360	This work
CCSD(T)/6-311+G(3df,2p)//B3LYP/6-311G(d,p)	366.9	Chin and Lee (2011)
(8e,7o)-CASPT2/pVDZ//CAS(8,7)/pVDZ	355.6	Fang (1999)
QCISD/pVDZ	373.6	Fang (1999)
CAS(8,7)/pVDZ	371.1	Fang (1999)
Methacrolein:		
B2GP-PLYP-D3	362	This work
G3X-K//M06-2X/6-31G(2df,p)	361.1	So et al. (2018)
Glyoxal → non-planar TS → H_2CO + CO:		
Experiment[b]	243	Saito et al. (1984)
B2GP-PLYP-D3/def2-TZVP	225	This work
G3	231.8	Koch et al. (2001)
MP2(full)/6-31+G(d)	256.9	Koch et al. (2001)
CBS-APNO//QCISD/6-311G(d,p)	227.6	Li and Schlegel (2001)
CCSD(T)/6-311+G(3df,2p)//B3LYP/6-311G(d,p)	232.6	Chin and Lee (2012)
Glyoxal → planar trans *TS → H_2CO + CO:*		
B2GP-PLYP-D3/def2-TZVP	320	This work
G3	324.7	Koch et al. (2001)
MP2(full)/6-31+G(d)	355.6	Koch et al. (2001)
CCSD(T)/6-311+G(3df,2p)//B3LYP/6-311G(d,p)	317.6	Chin and Lee (2012)
Glyoxal → planar cis *TS → H_2CO + CO:*		
B2GP-PLYP-D3/def2-TZVP	328	This work
G3	314.2	Koch et al. (2001)
MP2(full)/6-31+G(d)	344.8	Koch et al. (2001)
Glyoxal → HOCH + CO:		
B2GP-PLYP-D3/def2-TZVP	251	This work
G3	254.0	Koch et al. (2001)
MP2(full)/6-31+G(d)	276.1	Koch et al. (2001)
CBS-APNO//QCISD/6-311G(d,p)	249.8	Li and Schlegel (2001)
CCSD(T)/6-311+G(3df,2p)//B3LYP/6-311G(d,p)	253.3	Chin and Lee (2012)

a: Dunning's correlation consistent basis sets have been abbreviated pVNZ, for N = D,T,Q with 'a' representing the augmented basis set; CV represents core-valence corrections; *b*: low pressure high temperature limit.

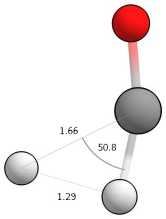

(a) Formaldehyde

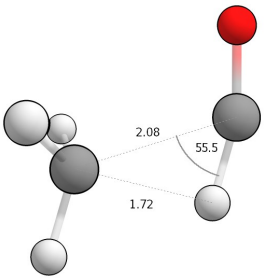

(b) Acetaldehyde

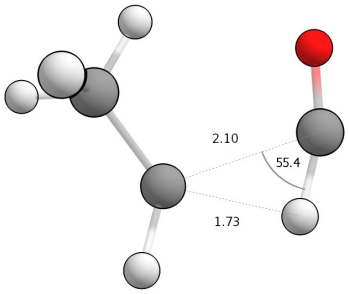

(c) Propanal

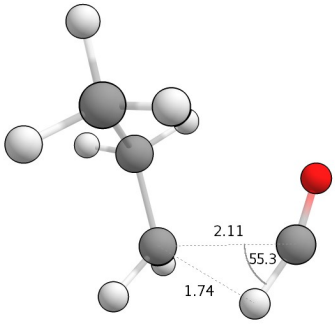

(d) Butanal

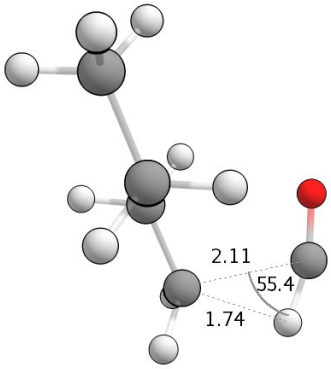

(e) Pentanal

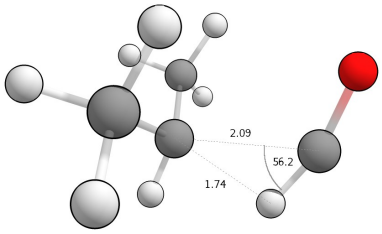

(f) 2-Methylpropanal

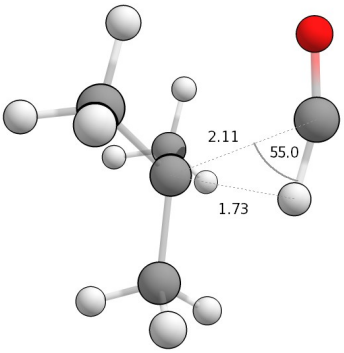

(g) 2,2-Dimethylpropanal

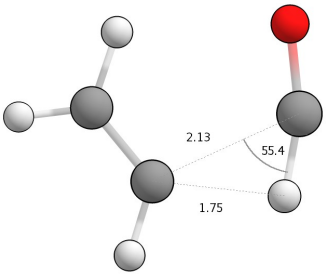

(h) Acrolein

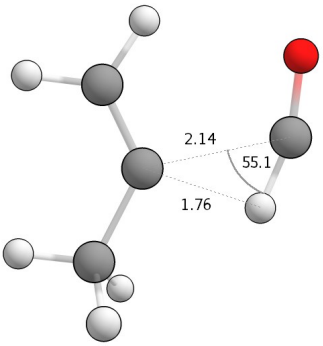

(i) Methacrolein

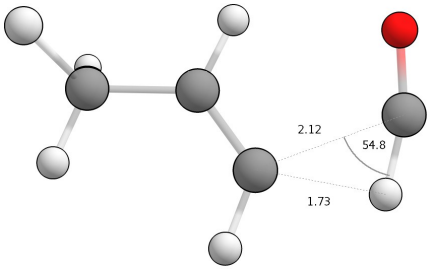

(j) Crotonaldehyde

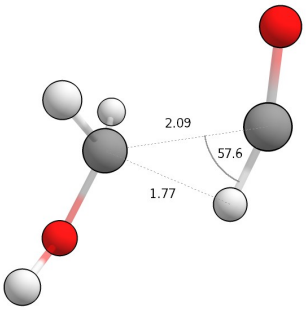

(k) Glycolaldehyde

Figure S2: B2GP-PLYP-D3/def2-TZVP transition state geometries for selected S_0 direct decarbonylation reactions.

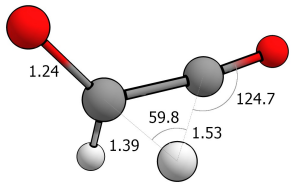

(a) Glyoxal → non-planar TS → H_2CO + CO

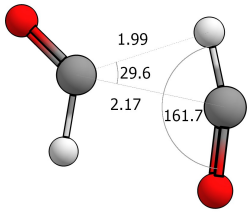

(b) Glyoxal → planar *trans* TS → H_2CO + CO

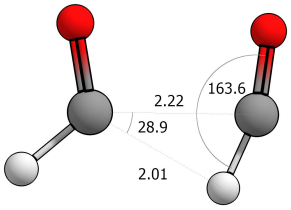

(c) Glyoxal → planar *cis* TS → H_2CO + CO

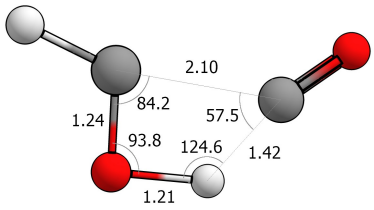

(d) Glyoxal → HOCH + CO

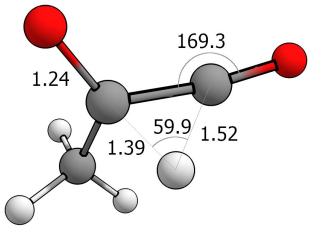

(e) Methylglyoxal → non-planar TS → CH_3CHO + CO

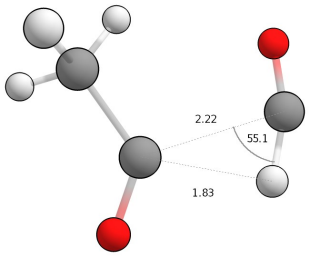

(f) Methylglyoxal → planar *trans* TS → CH_3CHO + CO

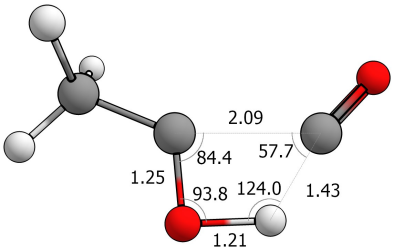

(g) Methylglyoxal → $HOCCH_3$ + CO

Figure S3: B2GP-PLYP-D3/def2-TZVP transition state geometries for S_0 direct decarbonylation reactions in glyoxal and methylglyoxal.

Methylglyoxal has similar decarbonylation pathways to glyoxal. First-order saddle points representing TSs for decarbonylation in methylglyoxal are also shown in Fig. S3. These pathways have not been previously reported and we calculate the lowest energy threshold, 235 kJ/mol, to be for decarbonylation to form acetaldehye, CH_3CHO, and CO via a "non-planar" TS, Fig. S3e, where the formyl H atom is out of the plane of the carbonyl groups. A *trans* planar TS for this reaction was also optimised, Fig. S3f, with corresponding threshold energy 333 kJ/mol. *trans*-Methylglyoxal can also dissociate to methylhydroxycarbene, $HOCCH_3$, and CO via a planar TS, Fig. S3g. We calculate this threshold energy to be 250 kJ/mol.

Figures S2 and S3 show that the TSs for decarbonylation are relatively 'late', that is, the breaking bond lengths are relatively long and the incipient product fragments have geometries approaching those in the isolated products. In particular, the C−C bond length is over 2 Å in all TSs. The key geometric parameters shown in Fig. S2 are also very similar for all carbonyls in the dataset and we expect this to be common to other atmospherically relevant aldehydes.

S3 Concerted triple fragmentation (TF) reactions

Aldehydes with a β hydrogen can undergo concerted TF to form H_2, CO and an unsaturated species. In molecules with two possible β hydrogen sites, there may be two concerted TF channels, for example, TF in methacrolein can form propyne, HC≡C–CH_3, H_2 and CO, or allene, H_2C=C=CH_2, H_2 and CO, with almost isoenergetic thresholds of 338 and 340 kJ/mol, respectively at B2GP-PLYP-D3/def2-TZVP. Note that only the lowest energy threshold is reported in Table 1 of the main text.

Triple fragmentation reactions have been studied theoretically for a few of the carbonyls in the dataset. Selected high-level literature results are shown in Table S2. Similarly to decarbonylation, threshold energies appear sensitive to the description of electron correlation and the quality of the geometry; the CASSCF(6,6) geometry does not appear adequate for propanal and the MP2/6-31+G(d) threshold for glyoxal appears anomalously high. Omitting these two values, the root-mean-square deviation of our calculated B2GP-PLYP-D3/def2-TZVP concerted TF thresholds to those in Table S2 is less than 9 kJ/mol. Notably, the G3X-K//M06-2X/6-31G(2df,p) thresholds of So et al. (2018) for the two TF channels in methacrolein are 15 and 13 kJ/mol higher than our B2GP-PLYP-D3/def2-TZVP values. We also predict a slightly lower energy threshold to TF to form HC≡C–CH_3 + H_2 + CO (338 kJ/mol), compared to H_2C=C=CH_2 + H_2 + CO (340 kJ/mol), whereas So et al. (2018) predict a 0.4 kJ/mol lower threshold to allene formation. There was, however, good agreement between our B2GP-PLYP-D3/def2-TZVP decarbonylation threshold in methacrolein and the G3X-K//M06-2X/6-31G(2df,p) result of So et al. (2018). Our calculated B2GP-PLYP-D3/def2-TZVP threshold is also ∼10 kJ/mol lower than the literature CCSD(T) result for acrolein (Chin and Lee, 2011).

First-order saddle points, representing TSs for the S_0 concerted TF reaction, are shown in Fig. S4. Key geometric parameters, in Å and degrees, are also shown in the figure. Note that only aldehydes with a β H atom can undergo concerted TF reaction.

Figure S4 shows that, like decarbonylation, the TSs for TF are 'late', resembling products. The large distances between incipient fragments suggest dispersion interactions are likely to be important in these TS and this underlies our use of the D3 dispersion correction. These non-bonded interactions are captured in molecular-orbital based methods, like CCSD(T), but may not be adequately described by the parametrisation of the M06-2X density functional. If this is the case, agreement between our calculated methacrolein decarbonylation threshold and the G3X-K//M06-2X/6-31G(2df,p) result of So et al. (2018) may be fortuitous. Alternately, our B2GP-PLYP-D3 calculations may over-correct for dispersion, particularly in conjugated species.

Table S2: Comparison of calculated zero-point vibrational energy corrected S_0 thresholds (kJ/mol) for concerted triple fragmentation reactions.

Species and Method	Threshold	Reference
Propanal:		
B2GP-PLYP-D3/def2-TZVP	295	This work
CCSD(T)/6-311+G(3df,2p)//B3LYP/6-311G(d,p)	302.1	Chin and Lee (2012)
(10e,9o)-CASPT2/6-311++G(d,p)//CASSCF(6,6)/6-311++G(d,p)	286.1	Tsai et al. (2014)
CCSD(T)/6-311++G(d,p)//CASSCF(6,6)/6-311++G(d,p)	296.2	Tsai et al. (2014)
Acrolein:		
B2GP-PLYP-D3/def2-TZVP	343	This work
CCSD(T)/6-311+G(3df,2p)//B3LYP/6-311G(d,p)	353.3	Chin and Lee (2011)
Methacrolein $\rightarrow$ *HC*$\equiv$*C–CH*$_3$ + *H*$_2$ + *CO:*		
B2GP-PLYP-D3/def2-TZVP	338	This work
G3X-K//M06-2X/6-31G(2df,p)	353.1	So et al. (2018)
Methacrolein $\rightarrow$ *H*$_2$*C*=*C*=*CH*$_2$ + *H*$_2$ + *CO:*		
B2GP-PLYP-D3/def2-TZVP	340	This work
G3X-K//M06-2X/6-31G(2df,p)	352.7	So et al. (2018)
Glyoxal:		
B2GP-PLYP-D3/def2-TZVP	247	This work
G3	255.6	Koch et al. (2001)
MP2(full)/6-31+G(d)	263.2	Koch et al. (2001)
CBS-APNO//QCISD/6-311G(d,p)	247.7	Li and Schlegel (2001)
CCSD(T)/6-311+G(3df,2p)//B3LYP/6-311G(d,p)	249.8	Chin and Lee (2012)

Where literature results employ high quality correlation methods and accurate geometries for aliphatic carbonyls, for example the calculations of Li and Schlegel (2001) on glyoxal, these results are in excellent agreement with our calculated thresholds.

With the exception of glyoxal and glycolaldehyde, the TSs for concerted TF have a 5-centre planar geometry, that is, the five atoms involved in the breaking and forming bonds lie in the same plane, with the O atom in the forming CO molecule also in this plane. The geometric parameters describing the forming H_2 and CO fragments, as well as the breaking bonds and the $\angle$C$-$C$-$C angle are similar in all optimised 5-centre TSs.

Glyoxal and Glycolaldehyde have non-planar TS structures, indicated by the green planes in Figs S4j and S4l. In glyoxal, the TS is 4-centred as both formyl H atoms combine to form H_2 and the additional steric strain in glyoxal forces non-planarity in the concerted TS. Methylglyoxal, however, can form a planar 5-centre TS. Although there is a 4-centred TS for TF in glycolaldehye, the lowest energy concerted TF threshold is for a 5-centred TS involving the formyl and β OH hydrogen, Fig. S4l. The additional flexibility afforded to rotation of the O$-$H bond in glycolaldehyde leads to a reduction in steric strain at the TS and, at 292 kJ/mol, the lowest calculated TF threshold of any species. This pathway has not been previously proposed for glycolaldehyde (Atkinson et al., 2006; Wallington et al., 2018; Bacher et al., 2001; Zhu and Zhu, 2010; So et al., 2015; Cui and Fang, 2011) and is the lowest energy dissociation threshold

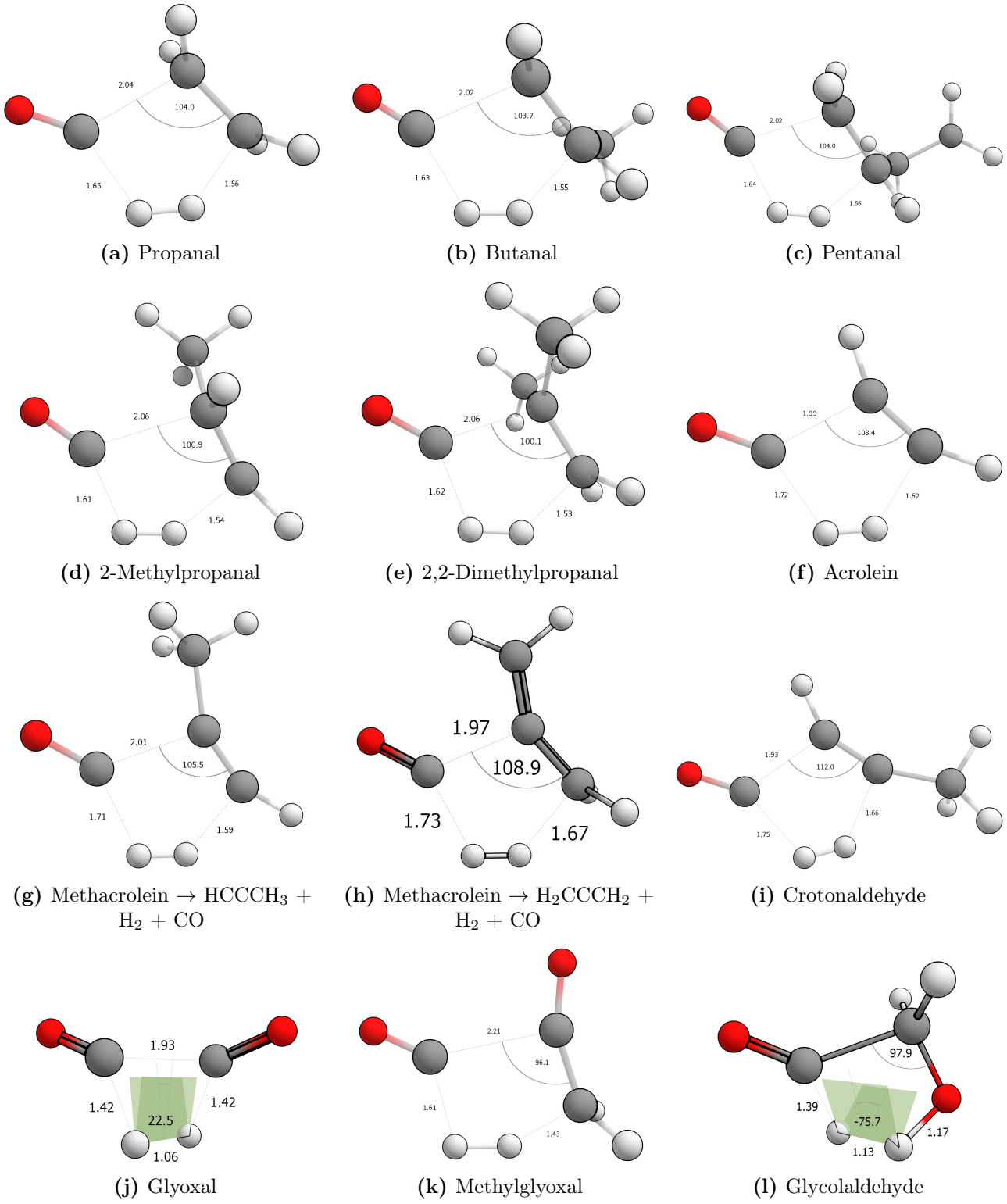

(a) Propanal **(b)** Butanal **(c)** Pentanal

(d) 2-Methylpropanal **(e)** 2,2-Dimethylpropanal **(f)** Acrolein

(g) Methacrolein → $HCCCH_3$ + H_2 + CO **(h)** Methacrolein → H_2CCCH_2 + H_2 + CO **(i)** Crotonaldehyde

(j) Glyoxal **(k)** Methylglyoxal **(l)** Glycolaldehyde

Figure S4: B2GP-PLYP-D3/def2-TZVP transition state geometries for S_0 concerted TF reactions.

we have found in glycolaldehyde. The Norrish type I reactions to form $^{\bullet}CH_2OH$ + $^{\bullet}CHO$ and $CH_2(OH)C^{\bullet}O$ + H have S_0 thresholds of 310 an 358 kJ/mol, respectively (Rowell et al. (2019)) and the O−H dissociation, to form $CH_2(O^{\bullet})CHO$ + $H^{\bullet}$ is at higher energy again. The other glycolaldehyde S_0 reactions: H_2–loss (292 and 384 kJ/mol), CO–loss (345 kJ/mol) and keto–enol tautomerisation (272 kJ/mol) also have higher thresholds than concerted TF.

S4 Norrish Type III reactions

Carbonyls with a β hydrogen can undergo NTIII reaction to form a smaller carbonyl and an unsaturated species. Similarly to concerted TF, where there are two distinct β hydrogens, there may be two possible NTIII channels. For example, NTIII in methacrolein can yield either propyne and formaldehyde or allene and formaldehyde with almost identical threshold energies of 379 and 382 kJ/mol, respectively at the B2GP-PLYP/def2-TZVP level of theory. Note that only the lowest energy threshold is included in Table 1 of the main text.

There are previous literature calculations of NTIII thresholds for propanal, acrolein and methacrolein, which are shown in Table S3. Similarly to TF, there is good agreement between our B2GP-PLYP-D3/def2-TZVP NTIII threshold and literature thresholds for propanal, although, similarly to TF, there are differences of 13–17 kJ/mol between the B2GP-PLYP-D3/def2-TZVP and literature thresholds in acrolein and methacrolein.

Table S3: Comparison of calculated zero-point vibrational energy corrected S_0 thresholds (kJ/mol) for NTIII reactions.

Species and Method	Threshold	Reference
Propanal:		
B2GP-PLYP-D3/def2-TZVP	332	This work
CBS-QB3	329.7	DeBoer and Dodd (2007)
G3	337.4	DeBoer and Dodd (2007)
Acrolein:		
B2GP-PLYP-D3/def2-TZVP	394	This work
CCSD(T)/6-311+G(3df,2p)//B3LYP/6-311G(d,p)	406.6	Chin and Lee (2011)
Methacrolein $\rightarrow$ $HCCCH_3$ + H_2CO*:*		
B2GP-PLYP-D3	379	This work
G3X-K//M06-2X/6-31G(2df,p)	395.8	So et al. (2018)
Methacrolein $\rightarrow$ H_2CCCH_2 + H_2CO*:*		
B2GP-PLYP-D3	382	This work
G3X-K//M06-2X/6-31G(2df,p)	397.1	So et al. (2018)

First-order saddle points, representing TSs for the S_0 NTIII reaction, are shown in Fig. S5. Key geometric parameters, in Å and degrees, are also shown in the figure.

Like those for direct decarbonylation and TF, the optimised TSs in Fig. S5 are relatively late, although there is steric strain in the four-membered CCCH rings. Despite this, key geometric parameters are remarkably conserved within each carbonyl class.

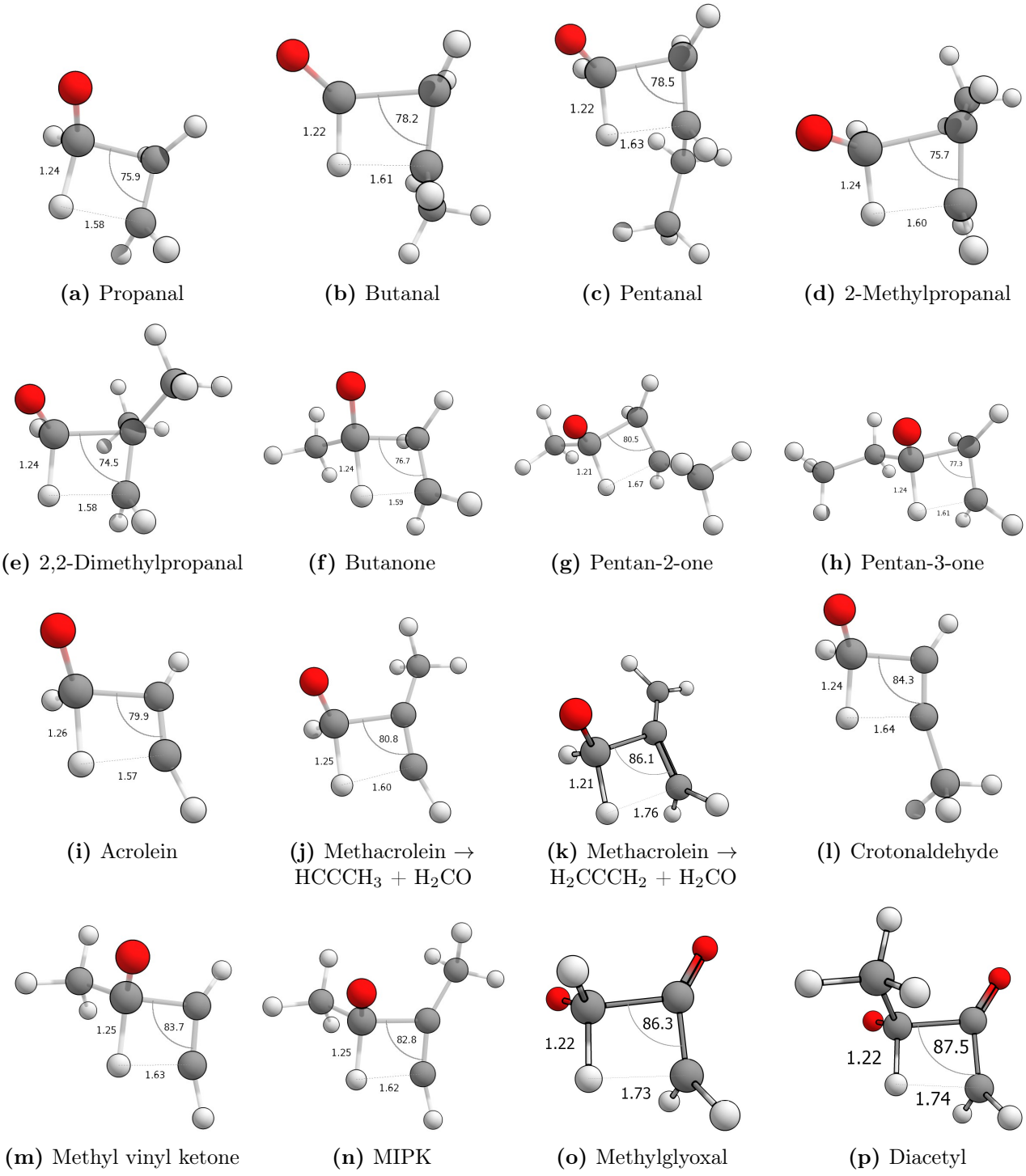

(a) Propanal **(b)** Butanal **(c)** Pentanal **(d)** 2-Methylpropanal

(e) 2,2-Dimethylpropanal **(f)** Butanone **(g)** Pentan-2-one **(h)** Pentan-3-one

(i) Acrolein **(j)** Methacrolein → $HCCCH_3 + H_2CO$ **(k)** Methacrolein → $H_2CCCH_2 + H_2CO$ **(l)** Crotonaldehyde

(m) Methyl vinyl ketone **(n)** MIPK **(o)** Methylglyoxal **(p)** Diacetyl

Figure S5: B2GP-PLYP-D3/deg2-TZVP transition state geometries for the S_0 Norrish Type III (β-H transfer) reactions.

S5 H_2–loss Reactions

Depending on size, the carbonyls in the dataset have a number of possible H_2–loss channels. Literature thresholds for the formyl + α H_2–loss channels are shown in Table S4. Our B2GP-PLYP-D3/def2=TZVP calculations compare well with the previous values for acetaldehyde and propanal with a ∼10 kJ/mol difference seen in acrolein.

Table S4: Comparison of calculated zero-point vibrational energy corrected S_0 thresholds (kJ/mol) for formyl + α H_2–loss reactions.

Species and Method[a]	Threshold	Reference
Acetaldehyde:		
B2GP-PYLP-D3/def2-TZVP	337	This work
G2	340.2	Martell et al. (1997)
CBS-QB3	339.7	Nguyen et al. (2005)
G3	341.4	Nguyen et al. (2005)
CCSD(T)/CBS//CCSD(T)/apVdDZ	336.4	Harding et al. (2007)
Propanal:		
B2GP-PLYP-D3/def2-TZVP	314	This work
CCSD(T)/6-311+G(3df,2p)//B3LYP/6-311G(d,p)	322.6	Chin and Lee (2012)
(10e,9o)-CASPT2/6-311++G(d,p)//CASSCF(6,6)/6-311++G(d,p)	314	Tsai et al. (2014)
Acrolein:		
B2GP-PLYP-D3/def2-TZVP	373	This work
CCSD(T)/6-311+G(3df,2p)//B3LYP/6-311G(d,p)	383.4	Chin and Lee (2011)

a: Dunning's augmented correlation consistent basis sets have been abbreviated pVNZ, for N = D,T,Q.

The B2GP-PLYP-D3/def2-TZVP optimised first order saddle points for H_2–loss reactions are provided as Cartesian coordinates in a ZIP folder.

S6 Alkane/alkene elimination

Analagous to the elimination of formyl and α-H atoms to form H_2 in aldehydes, an alkane can be eliminated in aliphatic ketones with an α hydrogen to form a ketene. In enones with an α hydrogen, the additional unsaturation leads to an alkene and a ketene.

This reaction has been previously reported in acetone (Saheb and Zokaie, 2018) and methyl vinyl ketone (So et al., 2018). These literature results are compared to our B2GP-PLYP-D3/def2-TZVP calculations in Table S5 and are within 4 kJ/mol of our calculated thresholds.

Table S5: Comparison of calculated zero-point vibrational energy corrected S_0 thresholds (kJ/mol) for alkane/alkene elimination reactions.

Species and Method	Threshold	Reference
Acetone:		
B2GP-PYLP-D3/def2-TZVP	363	This work
CCSD(T)/augh-cc-pVTZ+2df//MP2(full)/6-311+G(2d,2p)	367	Saheb and Zokaie (2018)
G4//MP2(full)/6-311+G(2d,2p)	367	Saheb and Zokaie (2018)
CBS-Q//MP2(full)/6-311+G(2d,2p)	367	Saheb and Zokaie (2018)
Methyl vinyl ketone:		
B2GP-PLYP-D3/def2-TZVP	329	This work
G3X-K//M06-2X/6-31G(2df,p)	332.6	So et al. (2018)

First-order saddle points, representing TSs for S_0 alkane/alkene elimination reactions in the ketones in our dataset are shown in Fig. S6. Key geometric parameters, in Å and degrees, are also shown in the figure. Asymmetric ketones, like butanone, have two possible alkane elimination pathways, both of which are indicated in the Fig. S6, along with their respective threshold energies. Note that only the lowest energy thresholds are reported in Table 1 of the main text.

In principle, methylglyoxal can also undergo alkane elimination to form methane, CH_4, and ethylenedione, O=C=C=O. The ethylenedione ground state, however, is a triplet biradical, analogous to molecular oxygen and the singlet species is dissociative to two CO molecules (Schröder et al., 1998). We were not able to optimise a first order saddle point for alkane elimination in S_0 methylglyoxal.

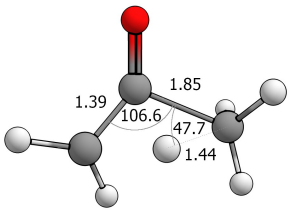

(a) Acetone → $H_2C{=}C{=}O + CH_4$ (363)

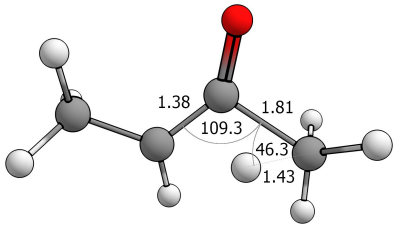

(b) Butanone → $CH_3HC{=}C{=}O + CH_4$ (351)

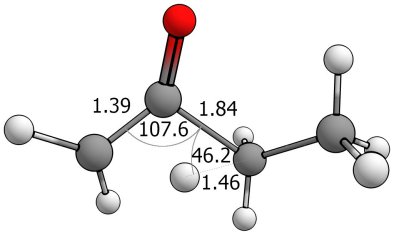

(c) Butanone → $H_2C{=}C{=}O + C_2H_6$ (363)

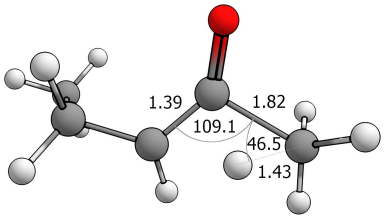

(d) Pentan-2-one → $C_2H_5HC{=}C{=}O + CH_4$ (347)

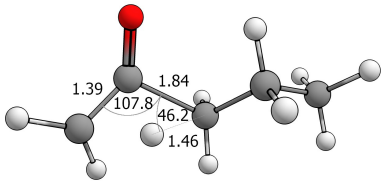

(e) Pentan-2-one → $H_2C{=}C{=}O + C_3H_8$ (358)

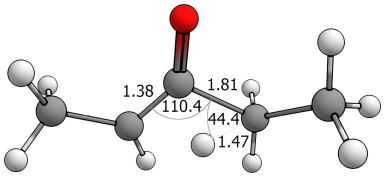

(f) Pentan-3-one → $CH_3HC{=}C{=}O + C_2H_6$ (347)

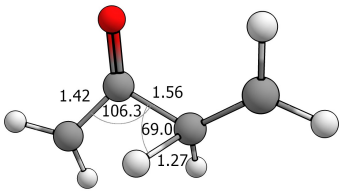

(g) Methyl vinyl ketone → $H_2C{=}C{=}O + C_2H_4$ (329)

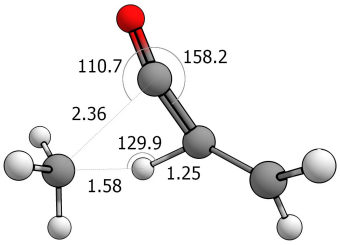

(h) Methyl vinyl ketone → $CH_4 + H_2C{=}C{=}C{=}O$ (388)

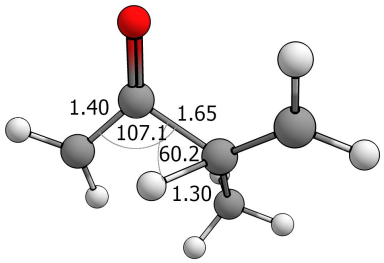

(i) Methyl isopropenyl ketone → $H_2C{=}C{=}O + C_3H_6$ (334)

Figure S6: B2GP-PLYP-D3/deg2-TZVP transition state geometries and zero-point corrected threshold energies (kJ/mol) for S_0 alkane/alkene elimination reactions.

S7 Keto–enol tautomerisation

Carbonyls with an α hydrogen can undergo a [1,2]-H atom shift and tautomerise to enols, where here 'keto' refers to both aldehydes and ketones. Calculations of keto–enol tautomerisation thresholds have been reported previously for a number of carbonyls in the dataset and are compared to our B2GP-PLYP-D3/def2-TZVP thresholds in Table S6.

In crotonaldehyde, a [1,5]-H atom shift involving a γ hydrogen is also possible, as shown in Fig. S7t. This is analogous to the [1,5]-H atom shift in an S_0 Norrish Type II reaction although, because it occurs in an enal, the C=C bond does not break but rather a conjugated dienol is formed. This threshold is also included in Table S6 and is predicted to be considerably lower in energy, at 133 kJ/mol, than the 294 kJ/mol threshold we predict for the [1,2]-H atom shift tautomerisation.

In glyoxal, a [1,2]-H shift can potentially form hydroxyketene and a [1,2]-H atom shift in methylglyoxal can potentially form hydroxymethylketene. We were unable to find first order saddle points for either tautomerisation, instead finding a saddle point for formation of hydroxymethylene, HOCH, and CO in glyoxal, with a threshold energy of 251 kJ/mol, and a saddle point for formation of methylhydroxycarbene, $HOCCH_3$, and CO in methylglyoxal, with a threshold of 250 kJ/mol. These reactions are considered in Section S2.

In general, our B2GP-PLYP-D3/def2-TZVP thresholds are in good agreement with literature calculations, although the threshold for acetone tautomerisation is lower than the previous calculations. In this case, however, it is clear that the threshold is sensitive to electron correlation and the CASPT2/6-31+G(d) results of Maeda et al. (2010) for acetone tautomerisation are unlikely to be reliable. Similarly to the previous thresholds, our calculated values for methyl vinyl ketone are ∼12 kJ/mol lower than the literature G3X-K//M06-2X/6-31G(2df,p) result. Note also that the MP2/cc-pVDZ energies of Elango et al. (2010) and the CCSD(T)/CBS+CV result for acetaldehyde (Shepler et al., 2008) do not include a zero-point vibrational energy correction and cannot be directly compared to the other thresholds. They have been included for the sake of completeness. Omitting these non-zero-point corrected values and the CASPT2/6-31+G(d) threshold for acetone, the root-mean-square deviation of our B2GP-PLYP-D3/def2-TZVP threhods to the literature values in Table S6 is <6 kJ/mol.

Many of the larger carbonyls in the dataset can have multiple enol isomers and only the lowest energy keto–enol threshold of each parent carbonyl is reported in Table 1 of the main text. The possible enol isomers include cases where the bulkier substituent is *cis* or *trans* to the forming OH substituent in the enol, or structural isomers if the parent carbonyl is an asymmetric

Table S6: Comparison of calculated zero-point vibrational energy corrected S_0 thresholds (kJ/mol) for keto–enol tautomerisation.

Species and Method[a]	Threshold	Reference
Acetaldehyde:		
B2GP-PYLP-D3/def2-TZVP	281	This work
G1	282	Smith et al. (1991)
CBS-QB3	283.3	Nguyen et al. (2005)
G3	282.4	Nguyen et al. (2005)
CCSD(T)/cc-pVTZ//B3LYP/6-311++G(d,p)	280.4	Yang et al. (2007)
CCSD(T)/CBS+CV[b]	296.2	Shepler et al. (2008)
Propanal → cis-prop-1-en-1-ol:		
B2GP-PLYP-D3/def2-TZVP	298	This work
MP2/pVDZ[b]	307	Elango et al. (2010)
CCSD(T)/apVTZ//B3LYP/6-31+G(d,p)	299	Shaw et al. (2017)
Propanal → trans-prop-1-en-1-ol:		
B2GP-PLYP-D3/def2-TZVP	278	This work
CBS-QB3	275.8	DeBoer and Dodd (2007)
G3	284.9	DeBoer and Dodd (2007)
MP2/pVDZ[b]	292	Elango et al. (2010)
CCSD(T)/apVTZ//B3LYP/6-31+G(d,p)	281	Shaw et al. (2017)
Acetone:		
B2GP-PLYP-D3/def2-TZVP	267	This work
(8e,7o)-CASPT2/6-31+G(d)	296.7	Maeda et al. (2010)
MP2/pVDZ[c]	282	Elango et al. (2010)
CCSD(T,full)/apVTZ//CCSD(T)/6-31+G(d,p)	273.4	Grajales-González et al. (2018)
CCSD(T)/ahpVTZ+2df//MP2(full)/6-311+G(2d,2p)[c]	273.6	Saheb and Zokaie (2018)
G4//MP2(full)/6-311+G(2d,2p)	275	Saheb and Zokaie (2018)
CBS-Q//MP2(full)/6-311+G(2d,2p)	277	Saheb and Zokaie (2018)
Crotonaldehyde [1,5]-H atom shift:		
B2GP-PLYP-D3/def2-TZVP	133	This work
B3LYP/6-311++G(d,p)	130.7	Wang et al. (2005)
B3LYP/6-311++G(3df,2p)	130.0	Wang et al. (2005)
MP2/6-311++G(3df,2p)	128.3	Wang et al. (2005)
Methyl vinyl ketone:		
B2GP-PLYP-D3/def2-TZVP	279	This work
G3X-K//M06-2X/6-31G(2df,p)	266.9	So et al. (2018)
Glycolaldehyde:		
B2GP-PLYP-D3/def2-TZVP	272	This work
G3X-K//M06-2X/6-31G(2df,p)	277.4	So et al. (2015)

[a]: Dunning's aug-cc-pVTZ and cc-pVTZ basis sets have been abbreviated apVTZ and pVTZ, respectively and CV indicates core-valence corrections; [b]: no zero-point vibrational energy correction; [c]: the ahpVTZ+2df basis set has additional high-exponent d- and f-type basis functions.

ketone. Asymmetric ketones have two distinct sites from which α-hydrogen transfer can occur. Thresholds for formation of the various isomers are provided in Table S7 for all relevant carbonyls, grouped by carbonyl class. The product enols are labelled with their systematic IUPAC names, for example, keto–enol isomerisation in acetaldehyde forms eth-1-ene-1-ol (vinyl alchohol). Note that we have not considered rotamers and, in general, only the lowest energy parent isomer was considered, for example, the *anti* conformer of acrolein. First-order saddle points, representing TSs for S_0 keto–enol tautomerisation are shown in Fig. S7. These are labelled by the enol

formed, with the parent carbonyl in parentheses. Key geometric parameters, in Å and degrees, are also shown in this figure.

Table S7: Zero-point vibrational energy corrected B2GP-PLYP-D3/def2-TZVP S_0 [1,2]-H atom shift keto–enol tautomerisation thresholds, by parent carbonyl class. (kJ/mol)

Aldehydes			**α,β-Unsaturated**		
Parent	Enol	Threshold	Parent	Enol	Threshold
Acetaldehyde	Eth-1-en-1-ol	281	Acrolein	Prop-1,2-dien-1-ol	291
Propanal	*cis*-prop-1-en-1-ol	297	Crotonaldehyde	But-1,2-dien-1-ol	294
Propanal	*trans*-prop-1-en-1-ol	278	Crotonaldehyde	But-1,3-dien-1-ol	133[a]
Butanal	*cis*-but-1-en-1-ol	298	Methyl vinyl ketone	But-1,2-dien-2-ol	282
Butanal	*trans*-but-1-en-1-ol	282	Methyl vinyl ketone	But-1,3-dien-2-ol	270
Pentanal	*cis*-pent-1-en-1-ol	297			
Pentanal	*trans*-pent-1-en-1-ol	281			
2-Methylpropanal	2-Methylprop-1-en-1-ol	296			
Ketones			**Carbohydrates**		
Parent	Enol	Threshold	Parent	Enol	Threshold
Acetone	Prop-1-en-2-ol	275	Glycolaldehyde	*cis*-eth-1-en-1,2-diol	323
Butanone	But-1-en-2-ol	275	Glycolaldehyde	*trans*-eth-1-en-1,2-diol	273
Butanone	*cis*-but-2-en-2-ol	294			
Butanone	*trans*-but-2-en-2-ol	274			
Pentan-2-one	Pent-1-en-2-ol	271			
Pentan-2-one	*cis*-pent-2-en-2-ol	286			
Pentan-2-one	*trans*-pent-2-en-2-ol	270			
Pentan-3-one	*cis*-pent-2-en-3-ol	294			
Pentan-3-one	*trans*-pent-2-en-3-ol	276			

a : threshold for [1,5]-H atom shift involving a γ hydrogen.

As seen in Table S7, thresholds to formation of *trans*-enols are typically ∼20 kJ/mol lower than those to the corresponding *cis*-enol. This can be rationalised by the steric penalty, which can be seen in Fig. S7, when the OH and bulkier substituent are on the same side of the enol double bond. There is a similar steric penalty for keto–enol tautomerisation of 2-methylpropanal, Fig. S7h, and this threshold energy is almost identical to that for forming the *cis*-enols.

In the asymmetric ketones, butanone and pentan-2-one, two distinct enols can be formed, although *cis* and *trans* isomers are only possible when the α hydrogen is from the non-methyl substituent (Figs S7k, S7l, S7n and S7o). In butanone, keto–enol tautomerisation to but-1-en-2-ol and *trans*-but-2-en-2-ol have almost identical thresholds, as does tauotomerisation of pentan-2-one to pent-1-en-2-ol and to *trans*-pent-2-en-2-ol (Table S7).

In α,β-unsaturated carbonyls, keto–enol tautomerisation can form substituted allenols (C=C=C(OH)R functionality): propadienol (allenol), but-1,2-dien-1-ol and but-1,2-dien-2-ol, which are relatively unstable. This is reflected in threshold energies of ∼290 kJ/mol. Methyl vinyl ketone can also transfer an aliphatic β H atom (Fig. S7u) to form a more stable conjugated diene, with a lower threshold energy of 270 kJ/mol.

Keto–enol tautomerisation in glycolaldehyde can occur with either α C−H to form an

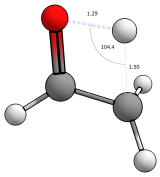

(a) Eth-1-en-1-ol (acetaldehyde)

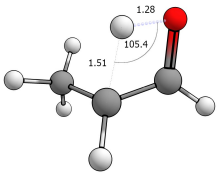

(b) *cis*-prop-1-en-1-ol (propanal)

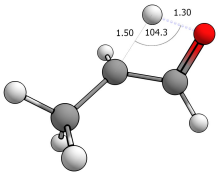

(c) *trans*-prop-1-en-1-ol (propanal)

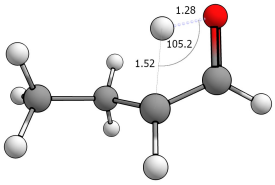

(d) *cis*-but-1-en-1-ol (butanal)

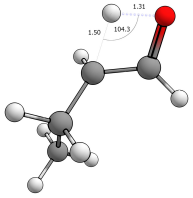

(e) *trans*-but-1-en-1-ol (butanal)

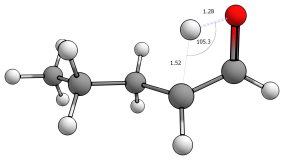

(f) *cis*-pent-1-en-1-ol (pentanal)

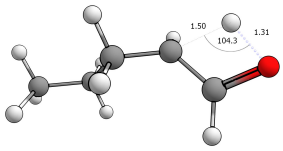

(g) *trans*-pent-1-en-1-ol (pentanal)

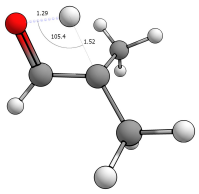

(h) 2-Methylprop-1-en-1-ol (2-methylpropanal)

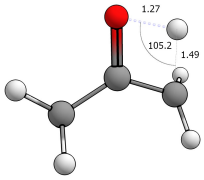

(i) Prop-1-en-2-ol (acetone)

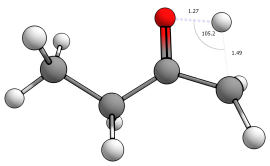

(j) But-1-en-2-ol (butanone)

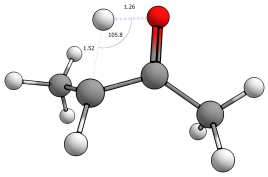

(k) *cis*-but-2-en-2-ol (butanone)

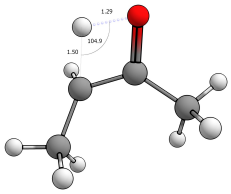

(l) *trans*-but-2-en-2-ol (butanone)

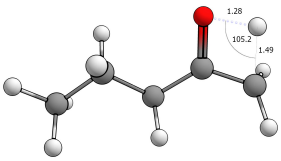

(m) Pent-1-en-2-ol (pentan-2-one)

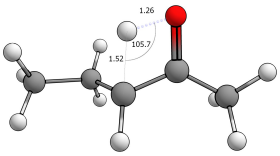

(n) *cis*-pent-2-en-2-ol (pentan-2-one)

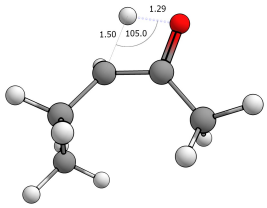

(o) *trans*-pent-2-en-2-ol (pentan-2-one)

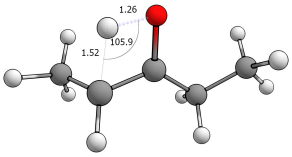

(p) *cis*-pent-2-en-3-ol (pentan-3-one)

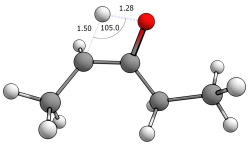

(q) *trans*-pent-2-en-3-ol (pentan-3-one)

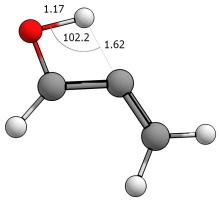

(r) Propadienol (acrolein)

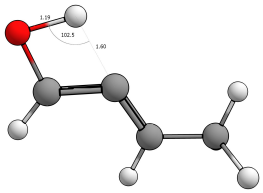

(s) But-1,2-dien-1-ol (crotonaldehyde)

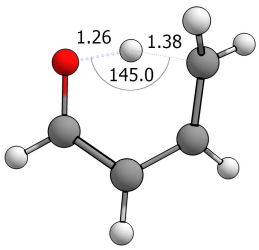

(t) But-1,3-dien-1-ol (crotonaldehyde)

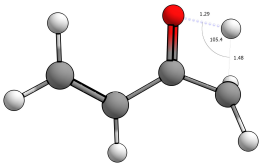

(u) But-1,3-dien-2-ol (methyl vinyl ketone)

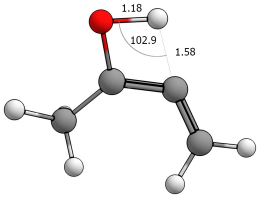

(v) But-1,2-dien-2-ol (methyl vinyl ketone)

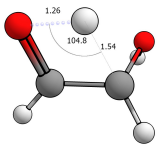

(w) *cis*-eth-1-en-1,2-diol (glycolaldehyde)

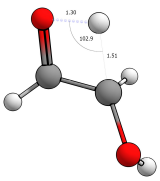

(x) *trans*-eth-1-en-1,2-diol (glycolaldehyde)

Figure S7: B2GP-PLYP-D3/def2-TZVP transition state geometries for S_0 keto–enol tautomerisation, labelled by the product enol with parent carbonyl in parentheses.

ethenediol where the two OH substituents are either *cis* or *trans*. As shown in Table S7, the threshold is 50 kJ/mol lower for formation of the *trans*-ethenediol; an OH group in the *cis* position has a greater energetic penalty than *cis* alkyl groups.

References

Atkinson, R., Baulch, D., and Cox: Evaluated kinetic and photochemical data for atmospheric chemistry: Volume II - gas phase reactions of organic species, Atmos. Chem. Phys., 6, 3625–4055, https://doi.org/https://doi.org/10.5194/acp-6-3625-2006, 2006.

Bacher, C., Tyndall, G. S., and Orlando, J. J.: The atmospheric chemistry of glycolaldehyde, J. Atmos. Chem., 39, 171–189, https://doi.org/10.1023/A:1010689706869, 2001.

Chin, C.-H. and Lee, S.-H.: Theoretical study of isomerization and decomposition of propenal, J. Chem. Phys., 134, 044 309, https://doi.org/10.1063/1.3521274, 2011.

Chin, C.-H. and Lee, S.-H.: Comparison of two-body and three-body decomposition of ethanedial, propanal, propenal, n-butane, 1-butene, and 1,3-butadiene, J. Chem. Phys., 136, 024 308, https://doi.org/10.1063/1.3675682, 2012.

Cui, G. and Fang, W.: Mechanistic photodissociation of glycolaldehyde: Insights from ab initio and RRKM calculations, ChemPhysChem, 12, 1351–1357, https://doi.org/10.1002/cphc.201000968, 2011.

DeBoer, G. D. and Dodd, J. A.: Ab initio energies and product branching ratios for the O + C_3H_6 Reaction, J. Phys. Chem. A, 111, 12 977–12 984, https://doi.org/10.1021/jp0755037, 2007.

Elango, M., MacIel, G. S., Palazzetti, F., Lombardi, A., and Aquilanti, V.: Quantum chemistry of C_3H_6O molecules: Structure and stability, isomerization pathways, and chirality changing mechanisms, J. Phys. Chem. A, 114, 9864–9874, https://doi.org/10.1021/jp1034618, 2010.

Fang, W.-H.: A CASSCF study on photodissociation of acrolein in the gas phase, Journal of the American Chemical Society, 121, 8376–8384, https://doi.org/10.1021/ja982334i, 1999.

Feller, D., Dupuis, M., and Garrett, B. C.: Barrier for the $H_2CO \rightarrow H_2$ + CO reaction: A discrepancy between high-level electronic structure calculations and experiment, J. Chem. Phys., 113, 218–226, https://doi.org/10.1063/1.481788, 2000.

Grajales-González, E., Monge-Palacios, M., and Sarathy, S. M.: Theoretical kinetic study of the unimolecular keto-enol tautomerism propen-2-ol↔ acetone. Pressure effects and implications in the pyrolysis of tert- and 2-butanol, J. Phys. Chem. A, 122, 3547–3555, https://doi.org/10.1021/acs.jpca.8b00836, 2018.

Harding, L. B., Klippenstein, S. J., and Jasper, A. W.: Ab initio methods for reactive potential surfaces, Phys. Chem. Chem. Phys., 9, 4055–4070, https://doi.org/10.1039/B705390H, 2007.

Karton, A., Tarnopolsky, A., Lamère, J.-F., Schatz, G. C., and Martin, J. M. L.: Highly accurate first-principles benchmark data sets for the parametrization and validation of density functional and other approximate methods. Derivation of a robust, generally applicable, double-hybrid functional for thermochemistry and thermochemical kinetics, J. Phys. Chem. A, 112, 12 868, https://doi.org/10.1021/jp801805p, 2008.

Koch, D. M., Khieu, N. H., and Peslherbe, G. H.: Ab initio studies of the glyoxal unimolecular dissociation pathways, J. Phys. Chem. A, 105, 3598–3604, https://doi.org/10.1021/jp0039013, 2001.

Li, X. and Schlegel, H. B.: Photodissociation of glyoxal: Resolution of a paradox, J. Chem. Phys., 114, 8–10, https://doi.org/10.1063/1.1336545, 2001.

Maeda, S., Ohno, K., and Morokuma, K.: A theoretical study on the photodissociation of acetone: Insight into the slow intersystem crossing and exploration of nonadiabatic pathways to the ground state, J. Phys. Chem. Lett., 1, 1841–1845, https://doi.org/10.1021/jz100551y, 2010.

Martell, B. J. M., Yu, H., and Goddard, J. D.: Molecular decompositions of acetaldehyde and formamide: theoretical studies using Hartree-Fock, Moller-Plesset and density functional theories, Mol. Phys., 92, 497–502, https://doi.org/10.1080/002689797170248, 1997.

Nguyen, T. L., Vereecken, L., Hou, X. J., Nguyen, M. T., and Peeters, J.: Potential energy surfaces, product distributions and thermal rate coefficients of the reaction of $O(^3P)$ with $C_2H_4(X^1A_g)$: A comprehensive theoretical study, J. Phys. Chem. A, 109, 7489–7499, https://doi.org/10.1021/jp052970k, 2005.

Polik, W. F., Guyer, D. R., and Moore, C. B.: Stark level-crossing spectroscopy of S_0 formaldehyde eigenstates at the dissociation threshold, J. Chem. Phys., 92, 3453–3470, https://doi.org/10.1063/1.457857, 1990.

Rowell, K. N., Kable, S. H., and Jordan, M. J. T.: Structural effects on the Norrish Type I α-bond cleavage of tropospherically important carbonyls, J. Phys. Chem. A, 123, 10 381–10 396, https://doi.org/10.1021/acs.jpca.9b05534, 2019.

Ruscic, B., Pinzon, R. E., Von Laszewski, G., Kodeboyina, D., Burcat, A., Leahy, D., Montoy, D., and Wagner, A. F.: Active thermochemical tables: Thermochemistry for the 21st century, J. Phys. Conf. Ser., 16, 561–570, https://doi.org/10.1088/1742-6596/16/1/078, 2005.

Ruscic, B. and Bross, D. H.: Active thermochemical tables (ATcT) values based on ver. 1.122p of the Thermochemical Network, URL `https://atct.anl.gov/`, 2020.

Saheb, V. and Zokaie, M.: Multichannel gas-phase unimolecular decomposition of acetone: Theoretical kinetic studies, J. Phys. Chem. A, 122, 5895–5904, https://doi.org/10.1021/acs.jpca.8b02423, 2018.

Saito, K., Kakumoto, T., and Murakami, I.: Thermal unimolecular decomposition of glyoxal, J. Phys. Chem., 88, 1182–1187, https://doi.org/10.1021/j150650a033, 1984.

Schröder, D., Heinemann, C., Schwarz, H., Harvey, J. N., Dua, S., Blanksby, S. J., and Bowie, J. H.: Ethylenedione: An intrinsically short-lived molecule, Chem. Eur. J., 4, 2550–2557, https://doi.org/10.1002/(SICI)1521-3765(19981204)4:12<2550::AID-CHEM2550>3.0.CO;2-E, 1998.

Shaw, M. F., Osborn, D. L., Jordan, M. J. T., and Kable, S. H.: Infrared spectra of gas-phase 1- and 2-propenol isomers, J. Phys. Chem. A, 121, 3679–3688, https://doi.org/10.1021/acs.jpca.7b02323, 2017.

Shepler, B. C., Braams, B. J., and Bowman, J. M.: "Roaming" dynamics in CH_3CHO photodissociation revealed on a global potential energy surface, J. Phys. Chem. A, 112, 9344–9351, https://doi.org/10.1021/jp802331t, 2008.

Smith, B. J., Nguyen, M. T., Bouma, W. J., and Radom, L.: Unimolecular rearrangements connecting hydroxyethylidene (CH_2-C-OH), acetaldehyde (CH_3-CH=O),and vinyl alcohol (CH_2=CH-OH), J. Am. Chem. Soc., 113, 6452–6458, 1991.

So, S., Wille, U., and Da Silva, G.: A theoretical study of the photoisomerization of glycolaldehyde and subsequent OH radical-initiated oxidation of 1,2-ethenediol, J. Phys. Chem. A, 119, 9812–9820, https://doi.org/10.1021/acs.jpca.5b06854, 2015.

So, S., Wille, U., and da Silva, G.: Photoisomerization of methyl vinyl Ketone and methacrolein in the troposphere: A theoretical investigation of ground-State reaction pathways, ACS Earth Space Chem., 2, 753–763, https://doi.org/10.1021/acsearthspacechem.8b00066, 2018.

Tsai, P.-Y., Hung, K. C., Li, H. K., and Lin, K. C.: Photodissociation of propionaldehyde at 248 nm: Roaming pathway as an increasingly important role in large aliphatic aldehydes, J. Phys. Chem. Lett., 5, 190–195, https://doi.org/10.1021/jz402329g, 2014.

Wallington, T. J., Ammann, M., Cox, R. A., Crowley, J. N., Herrmann, H., Jenkin, M. E., McNeill, V., Mellouki, A., and Troe, J.: IUPAC task group on atmospheric chemical kinetic data evaluation, URL `http://iupac.pole-ether.fr/`, 2018.

Wang, Y.-H., Zou, J.-W., Zhang, B., Lu, Y.-X., Jin, H.-X., and Yu, Q.-S.: EnoneâĂŞdienol tautomerism of but-2-enal and substituent effect: A theoretical study, J. Mol. Struct. THEOCHEM, 755, 31–37, https://doi.org/https://doi.org/10.1016/j.theochem.2005.06.029, 2005.

Yang, X., Maeda, S., and Ohno, K.: Insight into global reaction mechanism of [C2, H4, O] system from ab initio calculations by the scaled hypersphere search method, J. Phys. Chem. A, 111, 5099–5110, https://doi.org/10.1021/jp071238d, 2007.

Zhu, C. and Zhu, L.: Photolysis of glycolaldehyde in the 280–340 nm region, J. Phys. Chem. A, 114, 8384–8390, https://doi.org/10.1021/jp104497d, 2010.